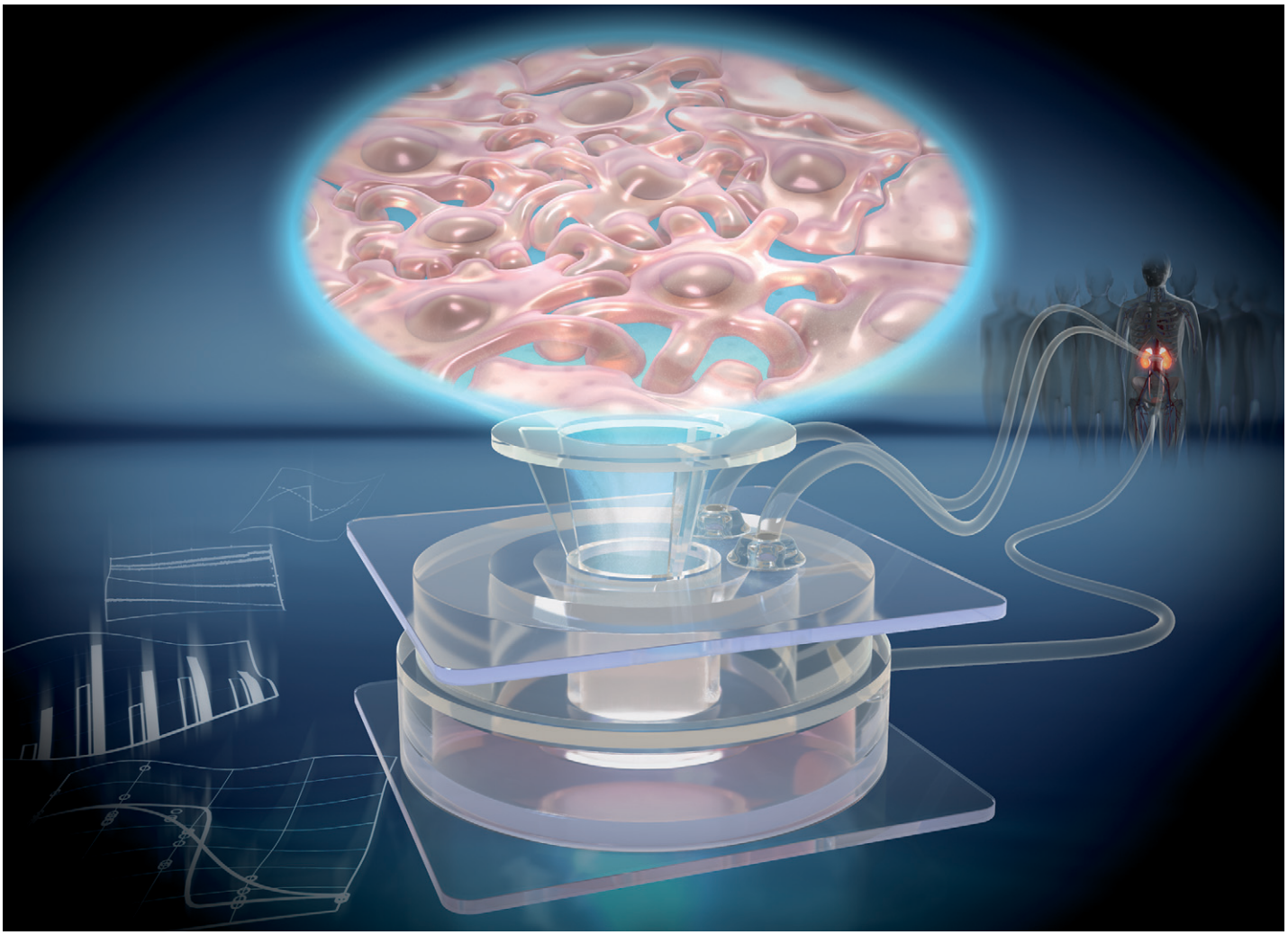

Featuring work from Applied Microfluidic Systems Laboratory of Professor Teruo Fujii, Institute of Industrial Science, the University of Tokyo, Tokyo, Japan.

Enhanced podocyte differentiation and changing drug toxicity sensitivity through pressure-controlled mechanical filtration stress on a glomerulus-on-a-chip

A microfluidic device that incorporates a commercially available culture insert has enabled precise control of filtration flow and user-friendly manipulation. The novel experimental setup with the device opens up novel insights into the mechano-stress biology of filtration flow on podocytes and advances glomerulus-on-a-chip research in the pursuit of overcoming kidney disease. This artwork was illustrated by Takashi Ando.

As featured in:

See Teruo Fujii *et al.*, *Lab Chip*, 2023, **23**, 437.

ROYAL SOCIETY OF CHEMISTRY

rsc.li/loc

Registered charity number: 207890

Lab on a Chip

PAPER

View Article Online
View Journal | View Issue

Cite this: *Lab Chip*, 2023, **23**, 437

Enhanced podocyte differentiation and changing drug toxicity sensitivity through pressure-controlled mechanical filtration stress on a glomerulus-on-a-chip†

Kotaro Doi, [a] Hiroshi Kimura, [b] Soo Hyeon Kim, [a] Shohei Kaneda, [c] Takehiko Wada, [d] Tetsuhiro Tanaka, [e] Akira Shimizu, [f] Takanori Sano, [a] Masamichi Chikamori, [a] Marie Shinohara, [a] Yukiko T. Matsunaga, [a] Masaomi Nangaku [g] and Teruo Fujii *[h]

Podocytes, localized in the glomerulus, are a prognostic factor of proteinuria in kidney disease and are exposed to distinct physiological stimuli from basal to apical filtration flow. Research studies on drug discovery and disease modeling for glomerulopathy have developed a glomerulus-on-a-chip and studied podocyte mechanobiology to realize alternative methods to animal experiments. However, the effect of filtration stimulus on podocytes has remained unclear. Herein, we report the successful development of a user-friendly filtration culture device and system that can precisely control the filtration flow using air pressure control by incorporating a commercially available culture insert. It allows mouse podocytes to be cultured under filtration conditions for three days with a guarantee of maintaining the integrity of the podocyte layer. Using our system, this study demonstrated that podocyte damage caused by hyperfiltration resulting from glomerular hypertension, a common pathophysiology of many glomerulopathies, was successfully recapitulated and that filtration stimulus promotes the maturation of podocytes in terms of their morphology and gene expression. Furthermore, we demonstrated that filtration stimulus induced different drug responsiveness in podocytes than those seen under static conditions, and that the difference in drug responsiveness was dependent on the pharmacological mechanism. Overall, this study has revealed differentiating and pharmacodynamic properties of filtration stimulus and brings new insights into the research field of podocyte mechanobiology towards the realization of glomerulus-on-a-chip.

Received 7th October 2022,
Accepted 5th December 2022

DOI: 10.1039/d2lc00941b

rsc.li/loc

Introduction

Podocytes are highly differentiated epithelial cells located at the outermost layer of the glomerular capillary wall. They are an important component of the permselective barrier in blood filtration, producing the glomerular basement membrane (GBM) in cooperation with glomerular endothelial cells (GEnCs).[1] Impairment of the permselective barrier in the glomerular capillary wall leads to the occurrence of proteinuria, resulting in glomerulopathy which can progress to end-stage kidney disease requiring renal replacement therapy. The function of the permselective barrier is of great interest in nephrology, as proteinuria is also an early indicator of asymptomatic glomerulopathies and is associated with total mortality.[2,3] Glomerulopathy is involved in the major pathophysiology of kidney disease, which affects one-tenth of the world's population and is associated with social problems including low quality of life, huge medical costs between $35 000 to $100 000 annually for end-stage kidney disease, and high mortality rates.[4]

Clinical practice guidelines that have improved the management of kidney disease, including glomerulopathy, such as the importance of salt reduction, weight control, and

[a] *Institute of Industrial Science, The University of Tokyo, Tokyo, Japan*
[b] *Micro/Nano Technology Center, Tokai University, Kanagawa, Japan*
[c] *Department of Mechanical Systems Engineering, Faculty of Engineering, Kogakuin University, Tokyo, Japan*
[d] *Division of Nephrology, Endocrinology and Metabolism, Tokai University School of Medicine, Kanagawa, Japan*
[e] *Department of Nephrology, Rheumatology and Endocrinology, Tohoku University Graduate School of Medicine, Miyagi, Japan*
[f] *Department of Analytic Human Pathology, Nippon Medical School, Tokyo, Japan*
[g] *Division of Nephrology and Endocrinology, The University of Tokyo Graduate School of Medicine, Tokyo, Japan*
[h] *The University of Tokyo, Tokyo, Japan. E-mail: tfujii@iis.u-tokyo.ac.jp*
† Electronic supplementary information (ESI) available. See DOI: https://doi.org/10.1039/d2lc00941b

strategies to suppress the renin–angiotensin–aldosterone system, have become prevalent in clinical practice over the past two decades.[5,6] Nevertheless, glomerulopathies remain a serious problem and little progress has been made in the development of therapies that improve patient prognosis, such as early decliner in diabetic kidney disease, primary focal segmental sclerosis, and Alport syndrome, where most patients progress to end-stage kidney disease.[7–10]

Animal experiments are mainstream in research on drug discovery related to glomerular toxicity and disease models of glomerulopathy as there were no useful *in vitro* tools that could assess permselective barrier function.[11–13] However, animal experiments have issues such as multi-organ effect, species differences with humans, individual differences, poor reproducibility, and increasing tendency for social exclusion.[14,15] Kidney organoids, which have been developed in the past decade, are also promising tools for assessing permselective barrier function, as they contain highly differentiated nephron component cells.[16–18] However, that function cannot be assessed due to the immaturity of the glomerular capillary structure.[19]

Various studies in the past decade have utilized glomerulus-on-a-chip (GoC), which aims to recapitulate the glomerular capillary wall by co-culturing podocytes and GenCs and evaluate the permselective barrier function in a microfluidic device.[20–28] GoC research, together with other organ-on-a-chip research,[29–33] has reported that a unique culture environment mimicking the *in vivo* physiological environment can elicit more potential in cultured cells than a conventional static culture, and thus is a promising alternative tool for animal experiments. Shear stress alone,[34] a combination of shear stress and a cyclic straining cell adherent substrate,[23] and a topographical micro-convex scaffold[25,35] have been reported to promote podocyte maturation through maturation marker expression and/or cellular process elongation of podocytes compared to conventional static culture.[36] Meanwhile, glomerular filtration flow is generated upon hemofiltration and is considered a vertical shear stress acting on the podocyte. It is distinct from horizontal shear stress because it is a force pulling away from the basal to the apical side for the cell. The mechanobiology of filtration flow, such as how it affects podocyte differentiation, is of interest; however, it has not been studied in detail.[37,38] Furthermore, the difference between drug sensitivity under physical stimulation and conventional static culture is a problem in drug discovery research that has not been studied in GoC.

Here, we have developed a user-friendly glomerular-mimicking filtration fluidic device (FFD) using a commercially available culture insert that can reproduce a precisely controlled vertical filtration flow by regulating the basal compartment pressure (P_{bc}) in the device. Using the FFD system, podocytes could be cultured for three days under filtration flow conditions with the optimized P_{bc}, maintaining the integrity of the podocyte layer, where the culture conditions promoted podocyte differentiation in terms of morphology and multiple maturation marker expression. Studies of disease conditions have demonstrated that hyperfiltration recapitulates the podocyte detachment and propagation of podocyte damage and that physical filtration stimulus alters the sensitivity of podocytes to toxic drugs, with the alterations varying according to pharmacological mechanisms.

Materials and methods

Filtration fluidic system

We designed the FFD system (Fig. 1C and D) to incorporate commercially available culture inserts with a removable format. To obtain reproducible performance from the filtration flow passing through the cell layer, we used culture inserts with a porous membrane certified as cell culture grade. An air phase in the basal compartment of the device allowed P_{bc} to be precisely controlled and monitored. The culture inserts were fixed in an airtight manner to the holder by means of an elastic sealing ring with the inside of the culture insert assigned to the apical compartment and the outside of the culture insert assigned to the basal compartment. Three independent tubes were applied to the basal compartment surrounded by the holder, one each for culture medium supply, air pressure regulation, and air pressure measurement, with a syringe pump (MFS-SP1, MFS Works, Tokyo, Japan), an air pressure regulator (MFS-APU1, MFS Works, Tokyo, Japan), and a pressure sensor (TruStability, Honeywell, Charlotte, NC, USA) connected to the origin of each tube. A gas filter (SLFGL25BS, Merck Millipore, Burlington, MA, USA) was inserted in the middle of the air pressure control and sensing lines to avoid bacterial contamination. To continuously record the sensed pressure, a pressure logging system (HSCDRRT Logger version 2.0, MFS Works, Tokyo, Japan) was connected to the pressure sensors.

For fabricating FFD, the top (Fig. S1Ab†) and bottom glass plates (Fig. S1Ac†) were made from glass slides (S9111, Matsunami, Osaka, Japan), which were cut with a glass knife and/or had holes cut using an ultrasonic abrasive grain processing machine (UM-2-7D, UE-100F20S-1B model, Ultrasonic Engineering Co., Ltd., Tokyo, Japan) for insertion of a culture insert and connection of two air-lines in the top glass plate. Silicone tubes (SR1554, Tigers Polymer Corporation, Osaka, Japan) were used for the three tubes (Fig. S1Ad†) connected to the basal compartment of the holder. A silicone tubing stabilizer (Fig. S1Ag†) was made by cutting a 2 mm thick polydimethylsiloxane (PDMS) (Silpot 184, DuPont Toray Specialty Materials K.K., Tokyo, Japan) plate into a cylinder with an inner diameter of 2 mm and an outer diameter of 4 mm, and then providing a skirt structure with non-cured PDMS glued to the outer side of the cylinder. The elastic seal (Fig. S1Ah†), top holder (Fig. S1Ai†), and bottom holder rings (Fig. S1Aj†) were made by curing the PDMS using aluminum molds with an acrylic plate lid (Fig. S1B†). All aluminum molds

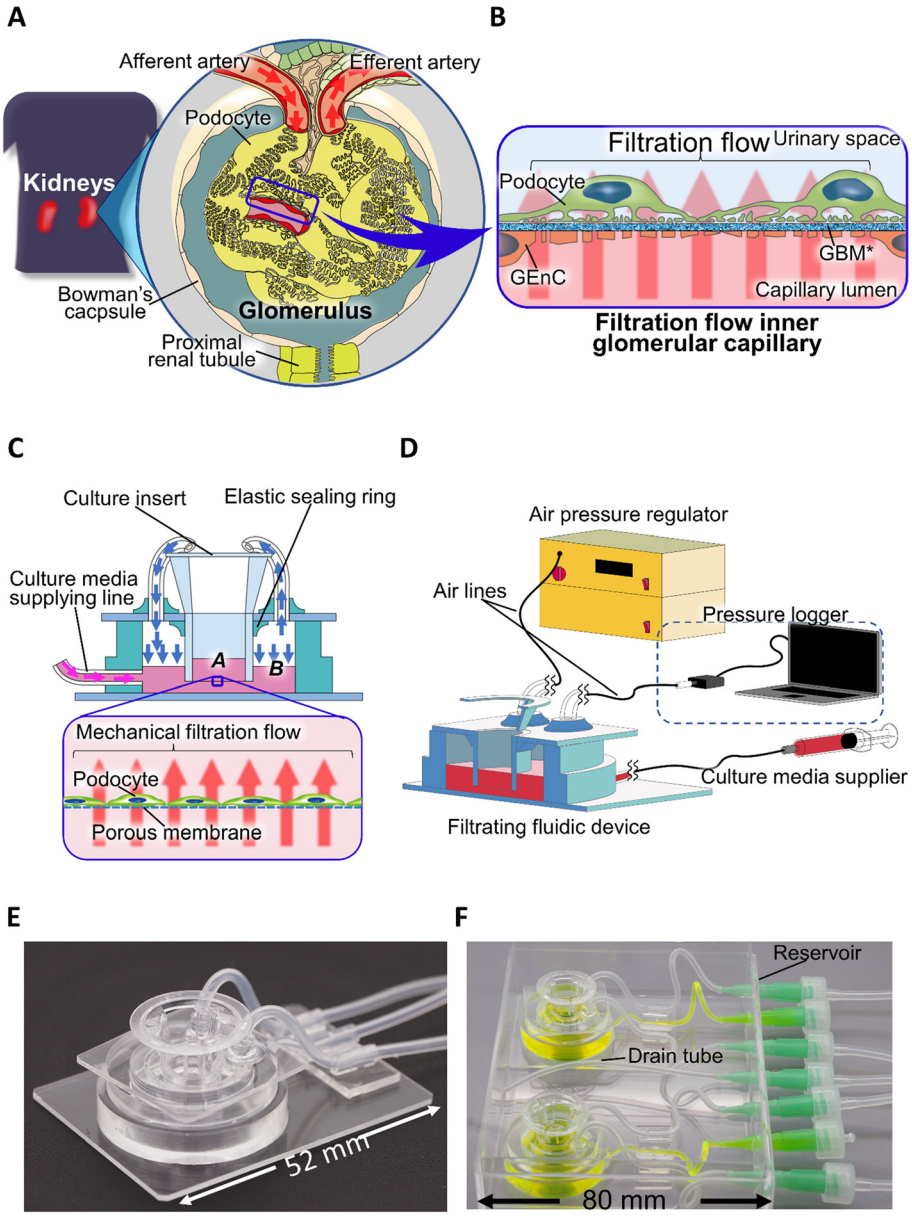

Fig. 1 Filtration flow in glomerulus and reproducing filtration mechanical stress with a filtration fluidic system. (A and B) Physiological filtration flow in the glomerulus. (A) Macro-structure of the glomerulus: the glomerulus is a ball-like mass of capillaries connected from the afferent artery and into the efferent artery encapsulated by Bowman's capsule. (B) Blood filtration flow acting on podocytes: the filtration flow is vertical and directed against the podocyte's adhesive substrate, flowing from the basal to the apical side. (C and D) The design of the filtration fluidic device and regulation system. (C) The design of the filtration fluidic device. A: apical compartment, B: basal compartment, pink arrow: culture medium supply, blue arrow: air pressure flow. (D) The configuration of the filtration system. (E and F) Real images of the filtration fluidic device. (E) Real image of the assembled filtration fluidic device. (F) Real image of the filtration fluidic device when culturing: two filtration fluidic devices were placed in a single dedicated package. The package includes a lid (not shown here) to avoid bacterial contamination and a drain tube for overflowing medium. The basal and apical compartments of the device are colored yellow and green, respectively.

were manufactured by machining an A5052 plate (Misumi, Tokyo, Japan). When bonding the components, oxygen plasma bonding (RIE-10NR, Samco, Kyoto, Japan) was used to bond PDMS to the glass, PDMS was glued to bond PDMS to PDMS and a silicone tube to PDMS. All PDMS curing procedures were performed at 75 °C for 120 min. FFDs, except for culture inserts, were sterilized by autoclave before use.

FFD mechanical actuation

To generate filtration flow in the FFD, two methods were compared: only medium supplied and direct regulation of P_{bc} assisted by medium supply. When the filtration flow was reproduced with only the medium supply, one of the air-lines was closed. When directly regulating P_{bc}, to keep the medium level constant in the basal compartment during the culture

filtration, the culture medium was supplied at a flow rate of 0.07 μL min^{-1}, 0.17 μL min^{-1}, and 0.35 μL min^{-1} for the P_{bc} conditions of 0.10 kPa, 0.25 kPa, and 0.50 kPa, respectively. In addition, the P_{bc} of all samples was measured every 5 min and recorded during filtration culture to demonstrate the actual P_{bc}.

Cell culture

Heat-sensitive mouse podocytes (HSMPs)[39] are conditionally immortalized mouse podocyte cell lines and were kindly gifted by the Shankland Lab at the University of Washington. Podocytes were grown in a basal medium consisting of RPMI 1640 medium (30264-85, Nacalai Tesque, Kyoto, Japan) containing 10% FBS (Sigma-Aldrich, St. Louis, MO, USA), with 100 U mL^{-1} penicillin, 100 μg mL^{-1} streptomycin (Thermo Fisher Scientific, Waltham, MA, USA), 1 mmol L^{-1} sodium pyruvate (Thermo Fisher Scientific, Waltham, MA, USA), and 10 mmol L^{-1} HEPES-KOH buffer (Dojindo Molecular Technologies, Kumamoto, Japan) in a 5% CO_2 incubator. Podocytes were propagated under permissive growth conditions at a temperature of 33 °C in the presence of 50 U mL^{-1} murine interferon-gamma (mIFNγ) (315-05, Peprotech, Cranbury, NJ, USA). Accutase (Nacalai Tesque, Kyoto, Japan) was used for cell dissociation in all the subculture processes.

Validation of the optimal extracellular matrix

Basement membrane matrix (Matrigel®) (354234, Corning, New York, USA), mouse type IV collagen (COL4) (354233, Corning, New York, USA), recombinant human laminin α5β1γ1 (L511) (NP892-012, Nippi, Tokyo, Japan) and recombinant human laminin α5β2γ1 (L521) (354221, Corning, New York, USA) were used to validate the optimal extracellular matrix (ECM) for podocytes. Matrigel diluted with RPMI 1640 medium, COL4 diluted with 0.05 mM HCl, L511 diluted with RPMI 1640 medium, and L521 diluted with RPMI 1640 medium were coated onto tissue culture-treated 48-well plates (3830, AGC Techno Glass, Tokyo, Japan) at a concentration of 1 μg cm^{-2} for Matrigel and COL4 and 0.1 μg cm^{-2} for L511 and L521 and incubated overnight at 4 °C according to the manufacturers' instruction. All ECM-coated wells were rinsed three times with FBS free medium consisting of Advanced RPMI 1640 medium (12633012, Thermo Fisher Scientific, Waltham, MA, USA) containing 10 mmol L^{-1} HEPES-KOH buffer and 2 mmol L^{-1} L-alanyl-L-glutamine, which was prepared for the ECM validating test to avoid the effect of cellular attachment factors included in FBS. Podocytes were seeded at a density of 4×10^4 cells per cm^2 in FBS free medium and cultivated under non-permissive growth conditions at 37 °C excluding IFNγ for four days. The control group was cultivated without ECM coating and in the basal medium. Phase contrast microscopy and cell viability analysis using WST-8 assay (the method is described in the WST-8 assay section) were performed to verify which ECMs would be most optimal to podocytes. The absorbance of the WST-8 assay for all groups was standardized to the control group.

Cell culture in the FFD

To transplant the podocytes into the FFD, podocytes were cultured in the culture insert (3470, Corning, New York, USA). Cells were seeded into the culture insert in the supplied 24-well plates. Prior to cell seeding, the porous membrane of the culture insert was coated with L521, selected based on the results of validation of optimal ECM (shown in Fig. S2†). Upon cell seeding, the culture insert was replaced with 100 μL of basal medium from L521 solution, then podocytes were seeded at a density of 1.5×10^5 cells per cm^2, resulting in a final medium volume of 300 μL in the culture insert. Podocytes in the culture insert were cultivated under non-permissive growth conditions with the 24-well plate in basal medium changed every other day and then transferred to the FFD three days after cell seeding.

TEER measurement

Transepithelial electrical resistance (TEER) was measured to assess the effect of filtration flow on podocyte barrier function before and after filtration (fluidic) culture with culture inserts set in 24-well plates using a Millicell® ERS-2 Voltohmmeter combined with STX03 electrodes (Merck Millipore, Burlington, MA, USA). The measured resistance was corrected to the surface area of the culture inserts and then subtracted from the resistance without cells. The pressure-dependent changes in podocyte barrier function due to filtration flow as a cell integrity marker was compared by subtracting the resistance before from the resistance after the filtration culture and then expressing the difference as a ratio to the static culture group.

WST-8 assay

A WST-8 assay was performed to verify the survival rate of the podocytes. WST-8 solution (Cell Counting Kit-8, Dojindo Molecular Technologies, Kumamoto, Japan) was mixed with basal medium at a ratio of 1 : 10. The mixed medium was replaced with the original medium at a volume of 110, 120, and 200 μL for the 96-well plates (3860, AGC Techno Glass, Tokyo, Japan), culture inserts, and 48-well plates, respectively, taking into account the culture surface area. Samples were incubated for four hours in a 5% CO_2 incubator, followed by collection of 100 μL of the reactive mixture into 96-well plates and absorbance was measured using a microplate reader (InfiniteF50R, TECAN, Männedorf, Switzerland).

Immunocytochemistry

Cultured cells in the culture inserts or multi-well plates were fixed with 4% paraformaldehyde in PBS for 10 min and subsequently permeabilized with 0.3% Triton X-100 in PBS for 5 min at room temperature. Anti-vimentin antibody (1 : 300) (ab92547, Abcam, Cambridge, UK) and Acti-stain 488

phalloidin (98 nM final concentration) (PHDG1-A, Cytoskeleton, Inc., Denver, CO, USA) were used to evaluate podocyte cytoskeletons. Primary antibody staining was performed *via* blocking preparation using an animal-free blocker (Vector Labs, Newark, CA, USA) diluted with Milli-Q water (1 : 5) overnight at 4 °C. Secondary antibody staining was performed using donkey anti-rabbit IgG and Alexa Fluor 568 (A10042, Thermo Fisher Scientific, Waltham, MA, USA) diluted with PBS together with Acti-stain and DAPI (1 : 1000) (D523, Dojindo Molecular Technologies, Kumamoto, Japan) overnight at 4 °C. Samples were washed with PBS after each antigen–antibody reaction at room temperature for 5 min three times. Anti-fading agents (ProLong Glass Antifade Mountant, P36980, Thermo Fisher Scientific, Waltham, MA, USA) were coated on both sides of the porous membrane, then culture inserts were incubated overnight at room temperature with a cover glass (2-176-08, Matsunami, Osaka, Japan) stuck to the bottom side of the porous membrane under light shielding.

Microscopy

Phase contrast images of cells cultured in 48-well plates were taken using an Olympus IX71N-22PH microscope. Fluorescence images were taken from the cell-free side of the porous membrane of the culture insert using a Keyence BZ-X700 fluorescence microscope with optical sectioning and Z-stack modes. Z-stacking images were processed using Fiji software v.1.53q.[40]

Scanning electron microscopy

Cells in culture inserts were fixed with 2.5% glutaraldehyde (Electron Microscopy Sciences, Hatfield, PA, USA) in 0.1 M phosphate buffer (pH 7.4) for two hours at room temperature followed by post-fixation with 1.0% osmium tetroxide (Electron Microscopy Sciences, Hatfield, PA, USA) in 0.1 M phosphate buffer (pH 7.4) for two hours and then dehydration in ascending grades (50%, 70%, 80%, 95% once for 10 min and 99.5% 3 times for 10 min) of ethanol. Samples were transferred to 100% *t*-butyl alcohol (Fujifilm Wako Pure Chemical Corporation, Osaka, Japan) for three changes and then frozen at −20 °C with a *t*-butyl freeze-drying device (VFD-21, Vacuum Device Co. Ltd., Ibararki, Japan). The cell-free side of the membrane of the culture inserts was fixed on an aluminum specimen mount (S-AM, Nisshin-EM, Tokyo, Japan) with carbon double-sided tape (7300, Nisshin-EM, Tokyo, Japan), and the non-membrane part of the culture insert was cut off using a 6 mm diameter biopsy punch (BP-L60K, KAI-Medical, Tokyo, Japan). Gold sputter coating was performed using a magnetron sputter (MSP-10, Vacuum Device Co. Ltd., Ibararki, Japan) immediately before observation. Scanning electron microscopy images were taken with an S-3000N instrument (Hitachi, Tokyo, Japan).

Transmission electron microscopy

The renal cortex tissues from 8-week-old C57BL/6 male mice were cut into small pieces and fixed in 2.5% glutaraldehyde in 0.1 M phosphate buffer at 4 °C overnight. The specimens were postfixed in 1% osmium tetroxide for four hours, dehydrated in ascending grades (50%, 70%, 80%, 95% once for 20 min and 99.5% 3 times for 20 min) of ethanol. The specimens were then embedded in propylene oxide (no. 311, Nisshin-EM, Tokyo, Japan), a substituting agent, for 10 min followed by incubation overnight in an equal mixture of propylene oxide and Epok 812 (02-1002, Okenshoji Co., Ltd., Tokyo, Japan), followed by the solidification of embedding resin consisting of EPOK812, DDSA (02-1005, Okenshoji Co., Ltd., Tokyo, Japan) and MNA (02-1006, Okenshoji Co., Ltd., Tokyo, Japan) at a ratio of 8 : 7 : 6 with DMP-30 (02-1009, Okenshoji Co., Ltd., Tokyo, Japan) at 1.5%. Serial ultrathin sections were cut using an ultra-cut S ultramicrotome (Leica, Wetzlar, Germany) with a diamond knife and picked up on nickel grids (Okenshoji Co., Ltd., Tokyo, Japan). The sections were double-stained with uranyl acetate and lead citrate. The sections were observed at 80 kV using H7650 (Hitachi, Tokyo, Japan).

All animal experiment protocols were approved by the Ethical Committee on Animal Experiments of the University of Tokyo (M-P16-125) and were conducted in accordance with institutional guidelines.

Quantitative real-time PCR

For RNA extraction, culture inserts of both the static and the fluidic groups were collected from FFDs into a 24-well cell culture plate after filtration culture. Cells in culture inserts were washed with 1 mL of serum-free RPMI 1640 culture medium before cell lysis. RNA extraction was performed using ReliaPrep™ RNA Miniprep Systems (Promega, Madison, WI, USA). RNA was reverse-transcribed into cDNA using ReverTra Ace® qPCR RT Master Mix (Toyobo, Osaka, Japan) and Veriti™ Thermal Cycler (Applied Biosystems, Waltham, MA, USA). Real-time PCR was performed using a THUNDERBIRD® SYBR® qPCR Mix (Toyobo, Osaka, Japan) and LightCycler® 96 System (Roche, Basel, Switzerland), with initial denaturation at 95 °C for 1 min followed by 40 cycles of 15 s at 95 °C, 30 s at 60 °C, and 45 s at 72 °C. The primers

Table 1 Primers used for quantitative RT-PCR

Gene		Sequence (5'-3')
GAPDH	F	AGGTCGGTGTGAACGGATTTG
	R	TGTAGACCATGTAGTTGAGGTCA
SYNPO	F	GGCCGATTGACAGAGCATCC
	R	TTCGGTGAAGCTTGTGCTCCG
PODXL	F	GCTGCTACTGTCGCCTGCAT
	R	TGTTGTGGCACTTTGGTGGCT
CD2AP	F	CCTCCTCCTGCAAAAGGTCC
	R	GCTTTGGGTACACTGCTCCA
VEGFA	F	GCACTGGACCCTGGCTTTAC
	R	ATCGGACGGCAGTAGCTTCG

used were designed using Primer-BLAST (NIH, Bethesda, MD, USA) and shown in Table 1. Expression levels of mRNA were expressed as a ratio of threshold cycle to GAPDH.

Podocyte toxicological sensitivity assay

Puromycin aminonucleoside (PAN) (169-20681, Fujifilm Wako Pure Chemical Corporation, Osaka, Japan) and doxorubicin hydrochloride (DOX) (D558000, Toronto Research Chemicals Inc, Toronto, ON, Canada), also known as Adriamycin, were employed to verify alterations in the drug sensitivity of podocytes by mechanical filtration stress. For dose–response experiments, PAN and DOX were dissolved in distilled water and then mixed with basal medium for five doses in serial dilutions (1.2 to 750 μM for PAN, and 0.01 to 100 μM for DOX). Cells in 96-well plates as the static culture condition and FFD as the fluidic culture condition were exposed to PAN and DOX in mixed medium three days after cell seeding, three days for PAN and one day for DOX, according to the protocol described in a previous report.[41] Under the fluidic culture condition, the medium in the culture insert was replaced with a drug-containing medium when the culture insert was transferred to the device.

The values of LD_{25}, LD_{50}, and LD_{75} were estimated by fitting the following four-parameter log-logistic model to three independent values under each experimental condition:

$$y = c + \frac{d - c}{1 + \exp(b(\log(x) - \log(LD_{50})))} \quad (1)$$

where y, x, LD_{50}, b, c, and d represent experimental data, the concentration of the drug, the median lethal dose, the slope at the median lethal dose, the lower-limit response, and the higher-limit response, respectively. These parameters and LD values were estimated and compared using the drc package[42] in R version 4.1.2.[43]

Statistical analysis

All values were obtained from multiple technical replicates using at least two biologically independent experiments. Student's *t*-test was used for comparisons between two groups. ANOVA with Tukey HSD test, Welch's ANOVA, and Kruskal–Wallis were performed for comparisons of three or more groups when the data set involved both normality and equivariance, normality only, and nonparametric, respectively. Differences were considered significant when $p < 0.05$.

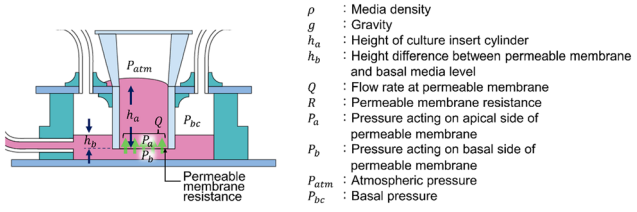

Fig. 2 Parameters related to filtration flow through the permeable membrane.

Results and discussion

Verification of the mechanical actuation method to precisely control filtration flow

To quantitatively evaluate the filtration flow in the FFD system, we clarified the relationship between individual parameters related to the filtration flow. The following equation, with reference to Darcy's law,[44] was used to identify the determinants that regulate filtration flow through the permeable membrane consisting of a porous membrane and a podocyte culturing layer (Fig. 2),

$$Q = \frac{P_b - P_a}{R} \quad (2)$$

where Q (m s^{-1}) is the filtration flow rate passing through the permeable membrane consisting of a porous membrane and cultured podocytes, P_a (Pa) and P_b (Pa) are the apical and basal pressure on the permeable membrane, respectively, and R (Ω sq^{-1}) is the resistance of the permeable membrane. Furthermore, P_a and P_b are formulated as follows.

$$P_a = \rho g h_a + P_{atm} \quad (3)$$

$$P_b = \rho g h_b + P_{bc} \quad (4)$$

where ρ (kg m^{-3}) is the density of the culture medium, g (m s^{-2}) is the gravitational acceleration, h_a (m) and h_b (m) are the water column heights from the porous membrane surface at the apical and basal compartment, respectively, and P_{atm} (Pa) and P_{bc} (Pa) are the pressures of the atmosphere and the basal compartment in the FFD, respectively. In practical experiments, P_{bc} (Pa) is the only factor that determines Q (m s^{-1}), as h_a (m) and h_b (m) are regarded as constant by initially filling the culture insert with culture medium and a certain medium supply in such a way that h_b (m) remains stable, respectively, and R (Ω sq^{-1}) is relatively invariant under the same culture conditions.

In comparing the methods of only supplying medium and directly regulating P_{bc} by supplying medium, the latter showed a constant measured P_{bc} with higher repeatability than the former (Fig. S3†). Hence, the method of directly controlling the P_{bc} in FFD using the air pressure regulator was employed to precisely control the filtration flow in this system.

Optimization of the extracellular matrix

The filtration flow in the basal to apical direction is a force for podocytes to be detached from the adhesive substrate in the FFD; thus the most optimal ECM as a scaffold should be selected. However, there has been no consensus on which ECM should be used in previously reported GoC[20,21,23,25,27,35] and podocyte mechanobiology studies.[34]

Phase contrast images of podocytes at day four under the culture conditions of each ECM demonstrated incomplete cellular growth in Matrigel and COL4, resulting in the apparent disaffinity of Matrigel and COL4 to podocytes (Fig. S2A†). Additionally, the WST-8 assay clarified that L521 had the highest absorbance ratio compared to the control group, significantly demonstrating the most optimal ECM of L521 to podocytes (Fig. S2B†), and thus, L521 was employed as a scaffold of podocytes.

This result is consistent with the fact that L521 is known to be a major ECM associated with integrin α3β1, one of the major focal adhesion molecules of podocytes, in the mature glomerular basement membrane.[45] The results also confirm that Matrigel and COL4, which were also used in previous GoC studies, are not optimal because of the major cellular attachment factors in them, type IV collagen α1α2 for COL4 and laminin α1β1γ1 for Matrigel,[46] which correspond to GBM components in early development.[47]

Optimization of mechanical filtration stress

To verify the optimal mechanical filtration flow, the integrity of the barrier function and cell adhesion, and the viability of podocytes were compared between P_{bc} conditions of 0.00 (static), 0.10, 0.25, and 0.50 kPa (Fig. 3A) with TEER measurement, immunocytochemistry, and WST-8 assay, respectively. The results of TEER (Fig. 3B) and WST-8 assays (Fig. 3C) demonstrated a peak at 0.10 kPa and a decrease above 0.25 kPa, meaning that the conditions above 0.25 kPa of P_{bc} tended to impair the integrity of the barrier function and viability compared to static conditions in a pressure-dependent manner. In addition, immunocytochemistry images from a macroscopic viewpoint (Fig. 3D) demonstrated that cell layer integrity was maintained up to 0.25 kPa, whereas at 0.50 kPa there were scattered areas of cellular detachment as indicated by yellow arrows, implying a breakdown of cell layer integrity with cell detachment. Taken together, we concluded that 0.10 kPa was a practical driving pressure for P_{bc}.

The practical driving P_{bc} was less than one-tenth of the *in vivo* glomerular effective filtration pressure (GEFP) of 1.3–3.0 kPa.[48] This is because the current filtration fluidic system lacks the glomerular basement membrane (GBM), which is considered to have the greatest pressure loss, based on the theory that the GEFP acts over three layers including glomerular endothelial cell, GBM, and podocyte.[49]

The increase in the WST-8 assay reflects increased mitochondrial activity rather than the number of viable cells.[50] Meanwhile, it has been reported that there is a correlation between mitochondrial activity and intercellular tight junction.[51] In consideration of these two findings, the present results suggest that the mitochondrial activity of podocytes was increased by filtration flow, as TEER tends to increase with the WST-8 assay under filtration conditions at 0.10 kPa.

Filtration pressure-dependent podocyte loss in the filtration fluidic device

Podocyte detachment from the GBM due to hyperfiltration is recognized as one of the major pathophysiological conditions

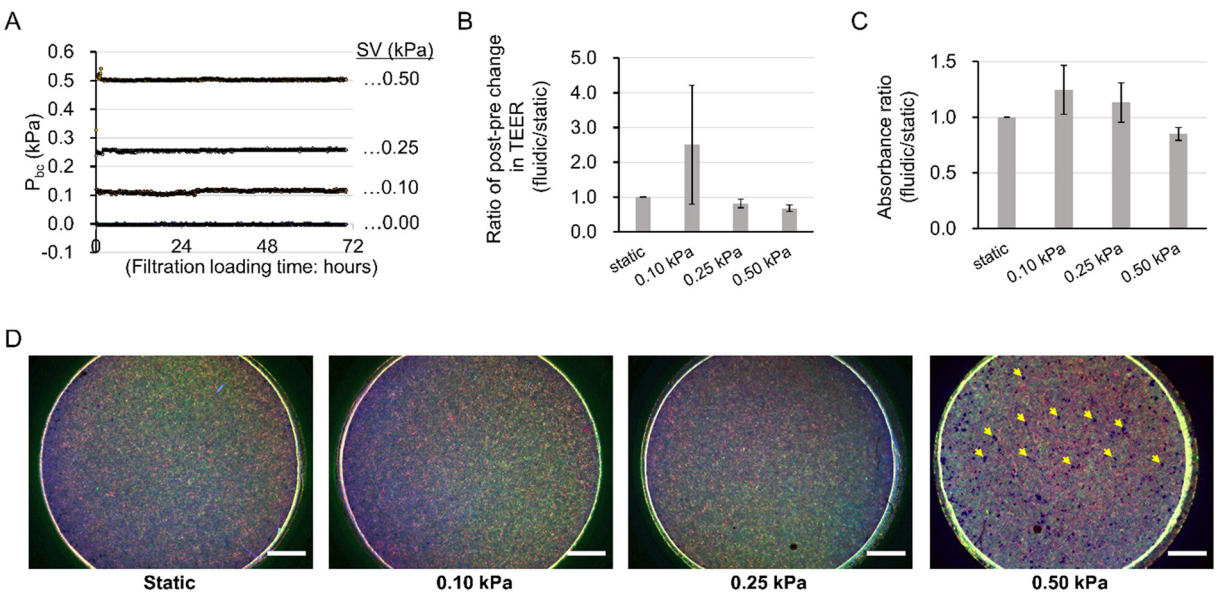

Fig. 3 Optimization of mechanical filtration strength. (A) Validated pressure conditions: pressure conditions of 0.50, 0.25, 0.10, and 0.00 (static) kPa in the basal compartment were validated. (B) Comparison of the post–pre changing ratio in transepithelial electrical resistance (TEER). Kruskal–Wallis test was performed to determine for significant differences between P_{bc} conditions. n = 3 independent samples. (C) Comparison of survival rates. Welch's ANOVA was performed to determine significant differences between P_{bc} conditions. n = 3 independent samples. (D) Integrity of cell layer after filtration culture. Vimentin (red), F-actin (green), and DAPI (blue), yellow arrows: cell detachment areas. Scale bars: 1000 μm.

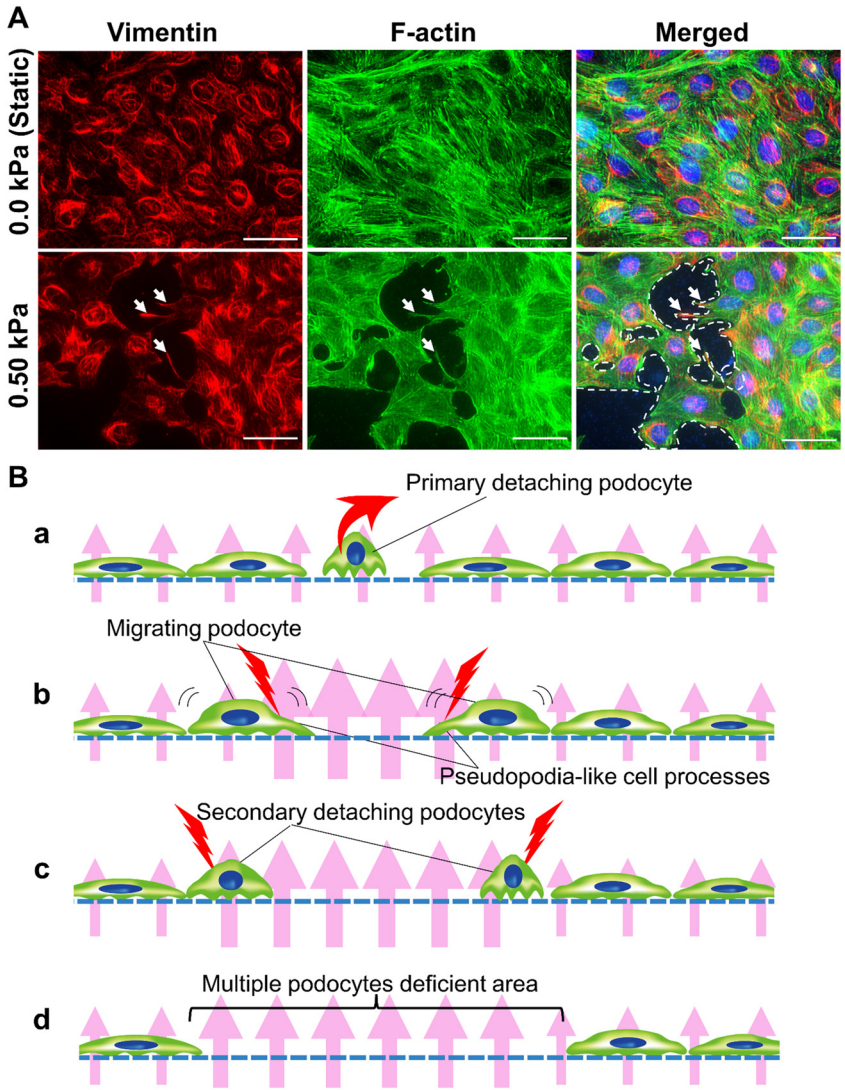

Fig. 4 Filtration pressure-dependent podocyte loss in the filtration device. (A) Immunofluorescence analysis of podocytes cultured under filtration flow conditions. Podocyte cytoskeletons were visualized by vimentin (vimentin, red) and F-actin (green). Under 0.50 kPa conditions, more podocyte-deficient areas (surrounded by the white dotted lines) were observed compared with static conditions. Many cell-deficient areas were large enough to be multiple cell adhesion areas. Cytoskeletal changes in vimentin and F-actin (white arrows) were observed in podocytes adjacent to areas of podocyte loss. Scale bars: 50 μm. (B) Podocyte damage propagation in FFD. (a) The most vulnerable podocytes were primary, detached by hyperfiltration. (b) A local increase of filtration flow velocity occurs in cell-deficient areas, and surrounding podocytes were more susceptible to damage from hyperfiltration. (c) Subsequently, secondary damaged podocytes were detached. (d) Consequently, multiple podocyte-deficient areas were formed.

in the development and progression of chronic kidney disease in hypertensive nephropathy.[52]

In experiments validating pressure conditions of P_{bc}, there was a significant difference in the number of cell-deficient regions between up to 0.25 kPa and 0.50 kPa. Therefore, we performed observations under 0.50 kPa filtration flow conditions at high magnification to examine the pathophysiology of podocyte detachment in podocyte injury based on cellular morphology.

Under the 0.50 kPa conditions, many cell-deficient areas were large enough to form multiple cell adhesion areas (surrounded by white dotted lines in Fig. 4A). Moreover, pseudopodia-like cell processes (white arrows in Fig. 4A), characterized by process structure with abundant vimentin and F-actin,[53] were observed in podocytes adjacent to the multicellular deficient areas, which might be a sign of cell migration that occurs in podocytes during nephrotic syndrome.[54]

The following pathophysiology can be inferred from these findings (Fig. 4B): primary single-cell detachment (Fig. 4Ba) causes the cells surrounding the detached cells to be susceptible to damage from hyperfiltration. Surrounding cells migrate with pseudopodia (Fig. 4Bb), resulting in secondary cell detachment (Fig. 4Bc) and a more enlarged area of cell defects (Fig. 4Bd).

Matsusaka *et al.* reported on the propagation of podocyte damage *in vivo*, where primary podocyte damage causes

secondary damage to surrounding podocytes. The authors hypothesized that the mechanism of podocyte damage propagation is due to the release of humoral factors that are toxic to podocytes, such as TGFβ, endothelin, and Wnt family members, from the primary damaged podocytes to the surrounding podocytes.[55]

Our results suggest that our developed FFD system not only mimics the pathophysiology of podocyte damage caused by pressure-dependent hyperfiltration but also reproduces podocyte damage propagation through the most common pathogenesis of glomerular injury – hyperfiltration. Propagation of podocyte damage is an important pathophysiology that causes the decrease in the number of podocytes per glomerulus leading to glomerulosclerosis;[56] thus this FFD system is informative as it is capable of providing an *in vitro* model of that pathophysiology.

Podocyte morphological differentiation by mechanical filtration stress

We examined the effect of 0.10 kPa filtration flow on podocyte morphology using a scanning electron microscopy approach. As shown in Fig. 5A, several process-like structures (green arrows) with branching (purple arrows in Fig. 5Ad) at intercellular junctions and arched transformation (yellow arrowheads in Fig. 5Ad) around the protruding parts of the process-like structure were observed under fluidic conditions, no such morphological changes were observed under static conditions.

The morphological hallmark of mature podocytes *in vivo* is a process formation with a three-dimensional architecture as shown in Fig. 5B. The podocyte cell body floats in Bowman's space, and the primary processes extend from the cell body and attach to the GBM while extending numerous secondary processes. Moreover, developmental studies of the kidney have shown that such morphological changes are observed after the initiation of filtration flow due to the fenestration of glomerular endothelial cells.[57,58] Considering these findings, our results indicate that filtration flow is one of the factors that characterize and maintain the podocyte morphology.

Korolj *et al.* and Xie *et al.* have previously reported that podocytes adhering to micro-convex topography elongate the foot processes of cultured podocytes.[25,35] However, they did not confirm the branching or three-dimensional arched transformation of foot processes observed in this study. Hence, this study elucidates a mechanobiology that cannot be revealed by micro-convex topography in terms of its impact on podocyte foot process formation.

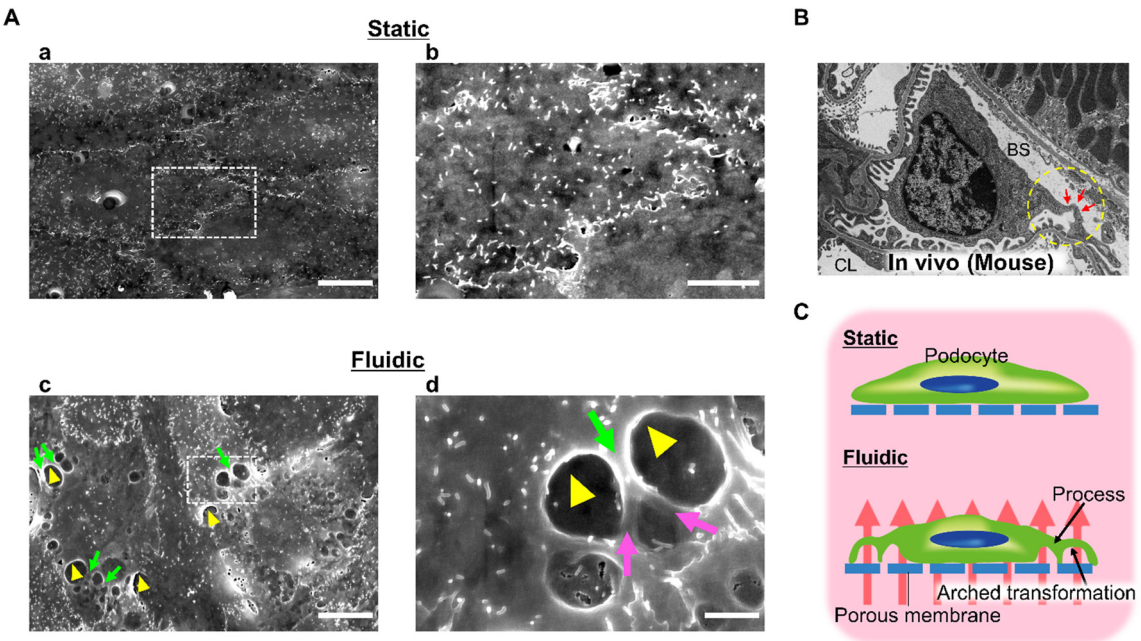

Fig. 5 Podocyte morphological differentiation from mechanical filtration stress. (A) Comparison of podocyte morphology between static and fluidic groups: podocytes in static (Aa and Ab) and fluidic (Ac and Ad) groups were observed by scanning electron microscopy. Ab and Ad are enlarged images of the white dotted boxed area in Aa and Ac, respectively. In the fluidic group, process-like morphological change (green arrows) was observed along the cell–cell junction with branching (purple arrows: Ad) at intercellular junctions and arched transformation perpendicular to the cellar basis of the porous membrane proved by cavities (yellow arrowheads) beneath the structure. The same morphological findings were not seen in the static group. Scale bars: 10 μm (Aa and Ac), 5 μm (Ab), 2 μm (Ad). (B) Podocyte morphology *in vivo* observed by transmission electron microscopy: the primary process extended from the margin of the cell body and formed the arched structure indicated by red arrows. CL, capillary lumen; BS, Bowman's space. (C) Hypothesis of the effect of mechanical filtration stimulation on podocyte morphology.

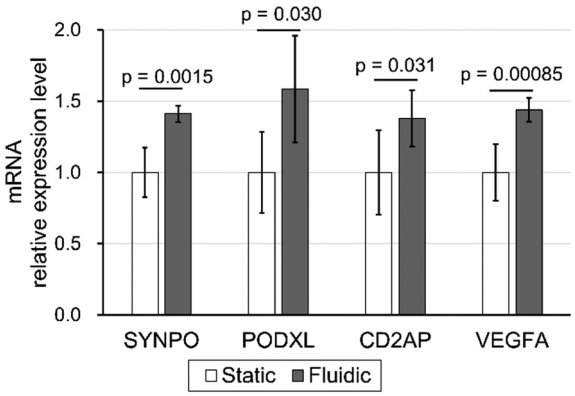

Fig. 6 Enhancement of podocyte differentiation markers of filtration mechanical stress. Podocyte maturation markers were quantified by real-time PCR and compared between static and fluidic groups. SYNPO, PODXL, CD2AP, and VEGFA expression levels were significantly higher in the fluidic condition than in the static condition (p-values by Student's t-test were 0.0015, 0.030, 0.031, and 0.00085, respectively). All data were normalized to GAPDH and shown as the ratio with the static condition expression level. Error bars represent standard deviation. n = 6 independent samples.

Enhancement of podocyte differentiation marker by filtration mechanical stress

Real-time PCR was performed to study the effect of filtration flow on podocyte differentiation. Synaptopodin (SYNPO), podocalyxin (PODXL), CD2AP, and VEGFA, podocyte differential markers, were compared between static and fluidic conditions with 0.10 kPa filtration flow, while NPHS1, NPHS2, and WT1 were excluded due to relative expression ratios to GAPDH of less than 0.005 (data not shown). All mRNA relative expression levels under fluidic conditions were significantly increased compared to static conditions (Fig. 6).

These results demonstrate that filtration, the vertical shear stress stimulus against the cell adhesion surface, promotes the expression of multiple podocyte differentiation markers. Moreover, based on the previous reports that SYNPO, PODXL, CD2AP, and VEGFA expression contributes to the maintenance of foot process structure in podocytes,[59–62] these results suggest that physical filtration stimuli have the potential to induce and maintain the process-like structure in podocytes, as shown in Fig. 5, *via* upregulated SYNPO, PODXL, CD2AP and VEGFA expression.

Yang *et al.* previously reported that fluid shear stress promoted the expression of multiple podocyte differentiation markers. However, the mechanism has yet to be addressed from a molecular biological perspective.[34] This study suggests that filtration flow may increase the mitochondrial metabolic activity in podocytes. Previous reports have also demonstrated that the mitochondrial metabolic activity of podocytes correlates with their differentiation.[63] Thus, the result suggests that filtration flow increased mitochondrial activity, which in turn increased mature podocyte markers.

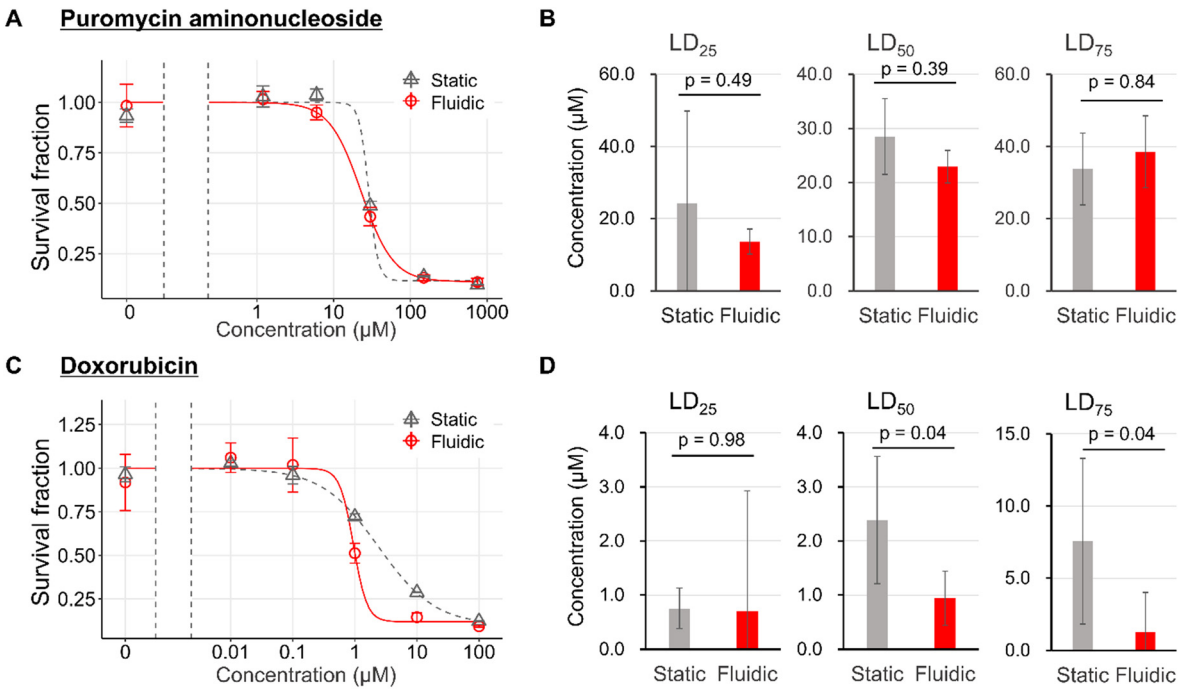

Fig. 7 Change in toxicological reactivity in podocytes from mechanical filtration stress. Dose–response curve of puromycin aminonucleoside (PAN) (A). LD_{25}, LD_{50}, and LD_{75} of PAN (B). Dose–response curve of doxorubicin (DOX) (C). LD_{25}, LD_{50}, and LD_{75} of DOX (D). Significant differences were determined by Student t-test based on 95% confidence intervals of the mean for each group: error bars represent standard error (A and C) or standard deviation (B and D) and n = 3 independent samples.

Change of toxicological reactivity in podocytes by mechanical filtration stress

Finally, we analyzed the effect of physical filtration stimulus of 0.10 kPa on the sensitivity of podocytes to toxic drugs. PAN and DOX were exposed to podocytes in the FFD system to examine the differences in drug toxicological sensitivity depending on the pharmacological mechanisms. Pharmacologically, PAN and DOX have been reported to have oxidative stress mechanisms on podocyte damage,[64,65] but the latter is recognized as more aggressive because it causes irreversible nephrosis after a single administration in animal experimental models. In contrast, PAN requires multiple administration[66] and has been reported to cause damage to cultured mouse podocytes at higher concentrations and in longer periods of time than DOX.[41]

In comparison between the static and the fluidic conditions, with regard to the pharmacodynamics of PAN, there were no significant differences in toxicant sensitivity between static and fluidic conditions (Fig. 7A and B). On the other hand, DOX demonstrated no difference at LD_{25}, and a significant leftward shift at LD_{50} and LD_{75} (Fig. 7C and D).

The LD_{50} of DOX in this study was considered to be significantly lower than the C_{max} of the mouse nephrotic model, based on the report by Lundgren-Eriksson *et al.*,[67] although it is not possible to mention PAN. This supposed divergence between *in vivo* and *in vitro* drug concentrations is due to the susceptibility to drug metabolism *in vivo*.

The reason for the leftward shift of fluidic conditions relative to static conditions in DOX might be that the filtration flow from the basal to the apical side exacerbated podocyte damage under toxic drug-induced injured conditions. The difference in the exacerbation of damage by filtration in DOX but not in PAN might be consistent, with DOX being more toxic to podocytes than PAN.[68,69]

Previous reports have shown that mechano-stress caused by medium flow has the potential to alter the drug response of cultured cells, which raises the issue of the inadequacy of conventional Petri dish-based static cell culture as an alternative drug discovery testing tool to animal experiments.[70,71] However, no studies have been conducted to date on cultured podocytes regarding changes in drug response due to mechano-stress. This study not only raises the issue of differences in drug sensitivity due to physical stimulus to static cultures, focusing on filtration flow to podocytes, but also shows that drug sensitivity differs depending on the pharmacological mechanism.

Conclusions

This study outlines the successful development of a user-friendly filtration culture system that allows precise control of filtration flow which enabled us to culture podocytes under filtration conditions for three days with a guarantee of maintaining the integrity of the podocyte layer. This system not only mimics podocyte damage caused by hyperfiltration but also reproduces a drug response different from that of static culture conditions while promoting podocyte maturation in morphology and gene expression.

The findings of this study were brought about by achieving two seemingly conflicting requirements employing removable culture inserts with an elastic ring: the airtightness for precise regulation of P_{bc} and the ease of access to cells exposed to filtration flow. The specification of the removable culture insert in pressure-controlled fluidic devices represents a higher user-friendliness in terms of bridging the two research fields of conventional life science research and organ-on-a-chip: compatibility with both approaches of conventional life science such as TEER measurement with fork-type electrodes, WST-8 assay, qPCR, and electron microscopy and organ-on-a-chip using mechanical filtration flow stimulation. This application, encouraged by its user-friendliness, will facilitate the validation of the mechanobiology by filtration flow in tissues with pressure-dependent molecular permeability, such as blood vessels, as well as other types of cultured podocytes.

In this study, the immortalized mouse podocyte was employed. As GoC research is essentially aimed at human drug discovery research and disease modelling, the mechanobiology of filtration flow should be examined in the future using human podocytes. In addition, although the co-culture of GEnCs with podocytes is possible by seeding and culturing GEnCs on the bottom side of the porous membrane prior to podocyte seeding, it was excluded to pursue the mechanobiology of podocytes by filtration flow in a simple system. However, this limitation, as well as reproducing the GBM structure, must be required to construct a filtration barrier with selective permeability to realize the practical application of GoC. In general, the filtration flow reproduced by a porous membrane is not as fine as that of the GBM, an *in vivo* ECM gel plate. Although the mechanobiology of podocytes with filtration flow through the ECM gel plate is inherently desired, innovation in integrating novel ECM gel biomaterials with both GBM components and rigidity to resist filtration flow into culture inserts will solve this limitation.

Furthermore, the differentiation of podocyte morphology by filtration flow shown in this study is not as fully differentiated as the interdigitating foot process formation observed *in vivo*. Under the conditions including highly interdigitated foot process formation, the responsiveness of podocytes to filtration flow is expected to significantly differ from that of the conventional cobblestone like morphology due to sub-podocyte space, increased surface area per podocyte, and slit diaphragm cell–cell junction. The mechanobiological insights from filtration flow based on such more sophisticated podocyte morphology will be useful for the practical application of GoC. A culture method to induce the interdigitating foot process formation of cultured podocytes has already been reported by several groups, including ours. Thus, this limitation will be resolved in the near future.

In the current filtration flow system, the dose–response curve of podocytes with filtration flow did not show a significant leftward shift of PAN. However, with the improvements of co-culture with GEnCs, reproducing GBM structure, and highly interdigitated foot processes formation, a significant leftward shift might occur. Furthermore, selective permeability tests with filtration flow and comparative verification of vertical and horizontal shear stresses should also be validated under such refined experimental conditions while developing mathematical models in collaboration with mathematicians for comparison with *in vivo* physiological data on filtration pressure and drug concentrations in the FFD system.

Overall, we are confident that the insights from this study into the mechanobiology of podocytes due to filtration flow will be of great benefit for the future practical application of GoC.

Author contributions

Conceptualization: K. D., H. K., S. H. K., S. K. and T. F. Methodology: K. D., H. K., S. H. K., S. K. and Y. T. M. Software: T. S. and M. C. Validation: K. D. Formal analysis: K. D., T. S. and M. C. Investigation: K. D., H. K., M. S. and Y. T. M. Resources: T. W. and A. S. Writing – original draft: K. D., H. K. and Y. T. M. Visualization: K. D. Supervision: T. W., T. T., A. S., M. N. and T. F. Project administration: M. N. and T. F. Funding acquisition: H. K., M. N. and T. F. All authors reviewed the manuscript.

Conflicts of interest

Kotaro Doi, Hiroshi Kimura, Masaomi Nangaku, and Teruo Fujii report a grant for patent number JP6968381B2. The authors declare the following financial interests/personal relationships which may be considered as potential competing interests: Kotaro Doi, Masaomi Nangaku, and Teruo Fujii received financial support from JSPS KAKENHI (Grant Number JP16K15464); Hiroshi Kimura from JSPS KAKENHI (Grant Number JP18H01849); and Kotaro Doi, Hiroshi Kimura, Masaomi Nangaku, and Teruo Fujii from AMED (Grant Number JP20be0304204) during the conduct of the study. The authors report no other conflicts of interest in this work.

Acknowledgements

We thank Arimi Ishikawa at the Department of Analytic Human Pathology, Nippon Medical School, for technically supporting the SEM experiment; Junichi Suehiro at the Department of Pharmacology and Toxicology, Kyorin University School of Medicine, for support on the statistical analysis of toxicity studies; and Microfluidic System Works Inc. for producing the air pressure regulator and pressure recording module. This work was partially supported by JSPS KAKENHI Grant Number JP18H01849 and JP16K15464, and the Japanese Agency for Medical Research and Development Grant Number JP20be0304204.

References

1 R. P. Scott and S. E. Quaggin, *J. Cell Biol.*, 2015, **209**, 199–210.
2 J. L. Gorriz and A. Martinez-Castelao, *Transplant. Rev.*, 2012, **26**, 3–13.
3 D. Y. Gaitonde, D. L. Cook and I. M. Rivera, *Am. Fam. Physician*, 2017, **96**, 776–783.
4 A. Levin, M. Tonelli, J. Bonventre, J. Coresh, J.-A. Donner, A. B. Fogo, C. S. Fox, R. T. Gansevoort, H. J. L. Heerspink, M. Jardine, B. Kasiske, A. Köttgen, M. Kretzler, A. S. Levey, V. A. Luyckx, R. Mehta, O. Moe, G. Obrador, N. Pannu, C. R. Parikh, V. Perkovic, C. Pollock, P. Stenvinkel, K. R. Tuttle, D. C. Wheeler and K.-U. Eckardt, ISN Global Kidney Health Summit participants, *Lancet*, 2017, **390**, 1888–1917.
5 A. Levin, B. Hemmelgarn, B. Culleton, S. Tobe, P. McFarlane, M. Ruzicka, K. Burns, B. Manns, C. White, F. Madore, L. Moist, S. Klarenbach, B. Barrett, R. Foley, K. Jindal, P. Senior, N. Pannu, S. Shurraw, A. Akbari, A. Cohn, M. Reslerova, V. Deved, D. Mendelssohn, G. Nesrallah, J. Kappel and M. Tonelli, *CMAJ*, 2008, **179**, 1154–1162.
6 A. K. Cheung, T. I. Chang, W. C. Cushman, S. L. Furth, F. F. Hou, J. H. Ix, G. A. Knoll, P. Muntner, R. Pecoits-Filho, M. J. Sarnak, S. W. Tobe, C. R. V. Tomson, L. Lytvyn, J. C. Craig, D. J. Tunnicliffe, M. Howell, M. Tonelli, M. Cheung, A. Earley and J. F. E. Mann, *Kidney Int.*, 2021, **99**, 559–569.
7 Y. Yoshida, K. Kashiwabara, Y. Hirakawa, T. Tanaka, S. Noso, H. Ikegami, M. Ohsugi, K. Ueki, T. Mita, H. Watada, D. Koya, K. Mise, J. Wada, M. Shimizu, T. Wada, Y. Ito, I. Narita, N. Kashihara, M. Nangaku and Y. Matsuyama, *BMJ Open Diabetes Res. Care*, 2020, **8**, e000902.
8 J. Kruegel, D. Rubel and O. Gross, *Nat. Rev. Nephrol.*, 2013, **9**, 170–178.
9 S. A. Carter, T. Gutman, C. Logeman, D. Cattran, L. Lightstone, A. Bagga, S. J. Barbour, J. Barratt, J. Boletis, D. Caster, R. Coppo, F. C. Fervenza, J. Floege, M. Hladunewich, J. J. Hogan, A. R. Kitching, R. A. Lafayette, A. Malvar, J. Radhakrishnan, B. H. Rovin, N. Scholes-Robertson, H. Trimarchi, H. Zhang, K. Azukaitis, Y. Cho, A. K. Viecelli, L. Dunn, D. Harris, D. W. Johnson, P. G. Kerr, P. Laboi, J. Ryan, J. I. Shen, L. Ruiz, A. Y.-M. Wang, A. H. K. Lee, S. Fung, M. K.-H. Tong, A. Teixeira-Pinto, M. Wilkie, S. I. Alexander, J. C. Craig and A. Tong, *Clin. J. Am. Soc. Nephrol.*, 2020, **15**, 673–684.
10 SONG-GD Initiative, S. A. Carter, L. Lightstone, D. Cattran, A. Bagga, S. J. Barbour, J. Barratt, J. Boletis, D. Caster, R. Coppo, F. C. Fervenza, J. Floege, M. Hladunewich, J. J. Hogan, A. R. Kitching, R. Lafayette, A. Malvar, J. Radhakrishnan, B. H. Rovin, H. Zhang, T. Gutman, M. Howell, C. Logeman, J. I. Shen, A. Teixeira-Pinto, S. I. Alexander, Y. Cho, J. C. Craig, D. Harris, D. W. Johnson, P. G. Kerr, J. Ryan, A. K. Viecelli, A. Y. M. Wang, M. Wilkie, N. Scholes-Robertson and A. Tong, *Kidney Int.*, 2019, **95**, 1280–1283.
11 J. A. Jefferson, J. W. Pippin and S. J. Shankland, *Drug Discovery Today: Dis. Models*, 2010, **7**, 27–33.

12 M. H. Foster, *Am. J. Physiol.*, 2016, **311**, F487–F495.
13 R. E. Cianciolo and J. C. Jennette, *Toxicol. Pathol.*, 2018, **46**, 898–903.
14 G. A. Van Norman, *JACC Basic Transl. Sci.*, 2019, **4**, 845–854.
15 K. Groff, E. Bachli, M. Lansdowne and T. Capaldo, *Environments*, 2014, **1**, 14–30.
16 R. Morizane, A. Q. Lam, B. S. Freedman, S. Kishi, M. T. Valerius and J. V. Bonventre, *Nat. Biotechnol.*, 2015, **33**, 1193–1200.
17 M. Takasato, P. X. Er, H. S. Chiu and M. H. Little, *Nat. Protoc.*, 2016, **11**, 1681–1692.
18 A. Taguchi and R. Nishinakamura, *Cell Stem Cell*, 2017, **21**, 730–746.e6.
19 S. Sharmin, A. Taguchi, Y. Kaku, Y. Yoshimura, T. Ohmori, T. Sakuma, M. Mukoyama, T. Yamamoto, H. Kurihara and R. Nishinakamura, *J. Am. Soc. Nephrol.*, 2016, **27**, 1778–1791.
20 M. Zhou, X. Zhang, X. Wen, T. Wu, W. Wang, M. Yang, J. Wang, M. Fang, B. Lin and H. Lin, *Sci. Rep.*, 2016, **6**, 31771.
21 L. Wang, T. Tao, W. Su, H. Yu, Y. Yu and J. Qin, *Lab Chip*, 2017, **17**, 1749–1760.
22 C. M. Sakolish and G. J. Mahler, *RSC Adv.*, 2017, **7**, 4216–4225.
23 S. Musah, A. Mammoto, T. C. Ferrante, S. S. F. Jeanty, M. Hirano-Kobayashi, T. Mammoto, K. Roberts, S. Chung, R. Novak, M. Ingram, T. Fatanat-Didar, S. Koshy, J. C. Weaver, G. M. Church and D. E. Ingber, *Nat. Biomed. Eng.*, 2017, **1**, 0069.
24 A. Petrosyan, P. Cravedi, V. Villani, A. Angeletti, J. Manrique, A. Renieri, R. E. De Filippo, L. Perin and S. Da Sacco, *Nat. Commun.*, 2019, **10**, 3656.
25 R. Xie, A. Korolj, C. Liu, X. Song, R. X. Z. Lu, B. Zhang, A. Ramachandran, Q. Liang and M. Radisic, *ACS Cent. Sci.*, 2020, **6**, 903–912.
26 C. Iampietro, L. Bellucci, F. O. Arcolino, M. Arigoni, L. Alessandri, Y. Gomez, E. Papadimitriou, R. A. Calogero, E. Cocchi, L. Van Den Heuvel, E. Levtchenko and B. Bussolati, *J. Pathol.*, 2020, **252**, 88–100.
27 Y. Roye, R. Bhattacharya, X. Mou, Y. Zhou, M. A. Burt and S. Musah, *Micromachines*, 2021, **12**, 967.
28 S. Y. Zhang and G. J. Mahler, *Micromachines*, 2021, **12**, 983.
29 J. Zhang, X. Wei, R. Zeng, F. Xu and X. Li, *Future Sci. OA*, 2017, **3**, FSO187.
30 H. Kimura, Y. Sakai and T. Fujii, *Drug Metab. Pharmacokinet.*, 2018, **33**, 43–48.
31 C. M. Sakolish, B. Philip and G. J. Mahler, *Biomicrofluidics*, 2019, **13**, 014107.
32 Q. Wu, J. Liu, X. Wang, L. Feng, J. Wu, X. Zhu, W. Wen and X. Gong, *J. Geophys. Res. Planets*, 2020, **19**, 9.
33 J. M. Donkers, H. Eslami Amirabadi and E. van de Steeg, *Curr. Opin. Toxicol.*, 2021, **25**, 6–14.
34 S. H. Yang, J. W. Choi, D. Huh, H. A. Jo, S. Kim, C. S. Lim, J. C. Lee, H. C. Kim, H. M. Kwon, C. W. Jeong, C. Kwak, K. W. Joo, Y. S. Kim and D. K. Kim, *Exp. Cell Res.*, 2017, **354**, 48–56.
35 A. Korolj, C. Laschinger, C. James, E. Hu, C. Velikonja, N. Smith, I. Gu, S. Ahadian, R. Willette, M. Radisic and B. Zhang, *Lab Chip*, 2018, **18**, 3112–3128.
36 K. Doi, H. Kimura, Y. T. Matsunaga, T. Fujii and M. Nangaku, *Int. J. Nephrol. Renovasc. Dis.*, 2022, **15**, 85–101.
37 T.-H. Chen, J.-S. Chen, Y.-C. Ko, J.-W. Chen, H.-Y. Chu, C.-S. Lu, C.-W. Chu, H.-H. Hsu and F.-G. Tseng, *Micromachines*, 2018, **9**, 228.
38 F. Schmieder, S. Behrens, N. Reustle, N. Franke, F. Sonntag, J. Sradnick and B. Hohenstein, *Curr. Dir. Biomed. Eng.*, 2019, **5**, 389–391.
39 S. V. Griffin, J. P. Olivier, J. W. Pippin, J. M. Roberts and S. J. Shankland, *J. Biol. Chem.*, 2006, **281**, 28048–28057.
40 J. Schindelin, I. Arganda-Carreras, E. Frise, V. Kaynig, M. Longair, T. Pietzsch, S. Preibisch, C. Rueden, S. Saalfeld, B. Schmid, J.-Y. Tinevez, D. J. White, V. Hartenstein, K. Eliceiri, P. Tomancak and A. Cardona, *Nat. Methods*, 2012, **9**, 676–682.
41 S. Chittiprol, P. Chen, D. Petrovic-Djergovic, T. Eichler and R. F. Ransom, *Am. J. Physiol.*, 2011, **301**, F660–F671.
42 C. Ritz, F. Baty, J. C. Streibig and D. Gerhard, *PLoS One*, 2015, **10**, e0146021.
43 *R: The R Project for Statistical Computing*, **https://www.r-project.org/**, (accessed July 5, 2022).
44 H. Darcy, *Les fontaines publiques de la ville de Dijon: exposition et application …*, Victor Dalmont, 1856.
45 R. Lennon, M. J. Randles and M. J. Humphries, *Front. Endocrinol.*, 2014, **5**, 160.
46 H. K. Kleinman and G. R. Martin, *Semin. Cancer Biol.*, 2005, **15**, 378–386.
47 D. R. Abrahamson, P. L. St. John, L. Stroganova, A. Zelenchuk and B. M. Steenhard, *J. Histochem. Cytochem.*, 2013, **61**, 706–718.
48 V. E. Andreucci, J. Herrera-Acosta, F. C. Rector and D. W. Seldin, *J. Clin. Invest.*, 1971, **50**, 2230–2234.
49 O. Smithies, *Proc. Natl. Acad. Sci. U. S. A.*, 2003, **100**, 4108–4113.
50 I. Lasocka, L. Szulc-Dąbrowska, M. Skibniewski, E. Skibniewska, K. Gregorczyk-Zboroch, I. Pasternak and M. Hubalek Kalbacova, *Materials*, 2021, **14**, 643.
51 V. Santa Cruz, T. R. Dugas and M. F. Kanz, *Toxicol. Sci.*, 2005, **84**, 129–138.
52 W. Kriz and K. V. Lemley, *J. Am. Soc. Nephrol.*, 2015, **26**, 258–269.
53 A. Ito, T. Mimae, Y.-S.-Z. Yamamoto, M. Hagiyama, J. Nakanishi, M. Ito, Y. Hosokawa, M. Okada, Y. Murakami and T. Kondo, *Lab. Invest.*, 2012, **92**, 1374–1385.
54 J. Reiser, J. Oh, I. Shirato, K. Asanuma, A. Hug, T. M. Mundel, K. Honey, K. Ishidoh, E. Kominami, J. A. Kreidberg, Y. Tomino and P. Mundel, *J. Biol. Chem.*, 2004, **279**, 34827–34832.
55 T. Matsusaka, E. Sandgren, A. Shintani, V. Kon, I. Pastan, A. B. Fogo and I. Ichikawa, *J. Am. Soc. Nephrol.*, 2011, **22**, 1275–1285.
56 M. Nagata, *Kidney Int.*, 2016, **89**, 1221–1230.

57 S. C. Satchell and F. Braet, *Am. J. Physiol.*, 2009, **296**, F947–F956.
58 K. Ichimura, S. Kakuta, Y. Kawasaki, T. Miyaki, T. Nonami, N. Miyazaki, T. Nakao, S. Enomoto, S. Arai, M. Koike, K. Murata and T. Sakai, *J. Cell Sci.*, 2016, jcs.187815.
59 L. Ning, H. Y. Suleiman and J. H. Miner, *Am. J. Physiol.*, 2021, **321**, F12–F25.
60 M. Barua, E. Shieh, J. Schlondorff, G. Genovese, B. S. Kaplan and M. R. Pollak, *Kidney Int.*, 2014, **85**, 124–133.
61 K. Tsuji, T. G. Păunescu, H. Suleiman, D. Xie, F. A. Mamuya, J. H. Miner and H. A. J. Lu, *Sci. Rep.*, 2017, **7**, 8321.
62 D. Veron, P. K. Aggarwal, Q. Li, G. Moeckel, M. Kashgarian and A. Tufro, *Front. Pharmacol.*, 2021, **12**, 788886.
63 Q. Yuan, J. Miao, Q. Yang, L. Fang, Y. Fang, H. Ding, Y. Zhou, L. Jiang, C. Dai, K. Zen, Q. Sun and J. Yang, *Cell Death Dis.*, 2020, **11**, 1–16.
64 C. B. Marshall, J. W. Pippin, R. D. Krofft and S. J. Shankland, *Kidney Int.*, 2006, **70**, 1962–1973.
65 R. Mohebbati, M. N. Shafei, M. Soukhtanloo, N. Mohammadian Roshan, A. Khajavi Rad, A. Anaeigoudari, S. Hosseinian, S. Karimi and F. Beheshti, *Avicenna J. Phytomed.*, 2016, **6**, 86–94.
66 V. W. S. Lee and D. C. H. Harris, *Nephrology*, 2011, **16**, 30–38.
67 L. Lundgren-Eriksson, A. Carlsson, S. Eksborg, W. Ryd, R. Vesanen and R. Hultborn, *Cancer Chemother. Pharmacol.*, 1997, **40**, 419–424.
68 R. L. Hall, W. L. Wilke and M. J. Fettman, *Toxicol. Appl. Pharmacol.*, 1986, **82**, 164–174.
69 A. Erdely, G. Freshour, C. Smith, K. Engels, J. L. Olson and C. Baylis, *Am. J. Physiol.*, 2004, **287**, F81–F89.
70 K.-J. Jang, A. P. Mehr, G. A. Hamilton, L. A. McPartlin, S. Chung, K.-Y. Suh and D. E. Ingber, *Integr. Biol.*, 2013, **5**, 1119–1129.
71 Y. A. Guerrero, D. Desai, C. Sullivan, E. Kindt, M. E. Spilker, T. S. Maurer, D. E. Solomon and D. W. Bartlett, *AAPS J.*, 2020, **22**, 53.